Electronic Supplementary Information (ESI†)

Atomic-Level Fe Doping in MoO_2/C Hollow Nanospheres for Enhanced Polysulfide Adsorption and Catalytic Conversion

Dongqing Xu[a], Jiajun Wei[a], Chenjie Yu[a], Wenqiang Lu[b], Yunfeng Chao[b], Jianhua Zhu[b*], Zhuosen Wang[b*], Xinwei Cui[b]

[a] Dongqing Xu, Jiajun Wei, Chenjie Yu,
College of Biomedical and Health, Anhui Science and Technology University, Fengyang 233100, Anhui, China

[b] Wenqiang Lu, Yunfeng Chao, Jianhua Zhu, Zhuosen Wang, Xinwei Cui
Henan Institute of Advanced Technology, Zhengzhou University, Zhengzhou 450052, P.R. China.
E-mail: jianhuazhu@zzu.edu.cn; zhuosenwang@zzu.edu.cn,

Experimental Section

Chemicals

Dopamine hydrochloride, ammonium molybdate tetrahydrate, m-dihydroxybenzene, sublimed sulfur, and potassium ferricyanide were purchased form Aladdin. All the reagents were analytical grade and used without further purification.

Synthesis of uniform Fe-Mo-polydopamine (PDA) precursor nanospheres:

Firstly, 500 mg $(NH_4)_6Mo_7O_{24}{\cdot}4H_2O$ was dissolved into 140 mL ultrapure water, then, 600 mg dopamine hydrochloride was added and stirring for 10 min, then 10 mg potassium ferricyanide was added. Subsequently, 300 mL absolute ethyl alcohol was poured into the above solution. After stirring for 30 min, ammonium hydroxides were added into the above solution and the pH value was adjusted to 8.5-9.0. Then the obtained mixture was stirred for another 4 h. Uniform Mo-PDA spheres were gained by filter and washed with ultrapure water and ethanol for three times, 80 C dry in vacuum oven overnight.

Synthesis of Mo-polydopamine (PDA) precursor nanospheres:

The synthesis procedure for Fe-MoO_2/C precursor nanospheres identical to the above process, except that no potassium ferricyanide source was added.

Synthesis of Fe-MoO_2/C and MoO_2/C hollow nanospheres:

The dried brown precursor powder was finely ground and then transferred into an

alumina boat, followed by pyrolysis in a tube furnace under an argon atmosphere at 650 °C for 4 h with a heating rate of 5 °C min^{-1}. The resulting black solid powder was collected as Fe-MoO_2/C and MoO_2/C.

Synthesis of Fe-MoO_2/C-S and MoO_2/C-S:

0.15 g of the obtained Fe-MoO_2/C-S or MoO_2/C-S and sublimed sulfur with a mass ratio 1:4 were mixed by grinding. Then the mixture was heated at 155 C for 12 h and cooled to room temperature. These composites were put into a porcelain boat, and heated to 200 C for 2 h in the quartz tube furnace under flowing Ar to evaporate the extra sulfur that exists outside the Fe-MoO_2/C or MoO_2/C.

Material characterization

An X-ray power diffractometer (XRD, Rigaku-DMax 2400) was used to obtain the phase information of the host materials and Cu Kα radiation flux at a scanning rate of 0.1° s^{-1}. Scanning electron microscopy (SEM) (Carl Zeiss Supra 40) and transmission electron microscopy (TEM) (JEM-2100F) were used to obtain structural and morphological information.

Electrochemical measurements

All the test CR2032 batteries were assembled in an Ar-filled glovebox in which both the O_2 and H_2O content < 0.1 ppm. The separator used a Celgard 2400 membrane, and the counter electrode used Li foil. The electrolyte was 1M lithium bis-(trifluoromethanesulfonyl) imide (LiTFSI) dissolved in 1,3-dioxolane (DOL)/diglyme (DME) (volume ratio of 1:1) with 2.0 wt% $LiNO_3$. The electrochemical performance was carried out by a battery test system (Neware CT4008T) from 1.7 V to 2.8 V.

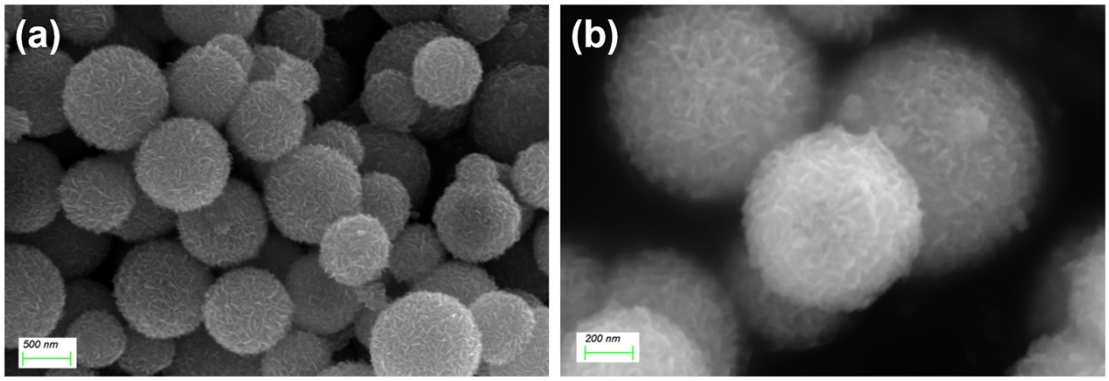

Fig. S1 SEM images of Fe-Mo PDA precursor

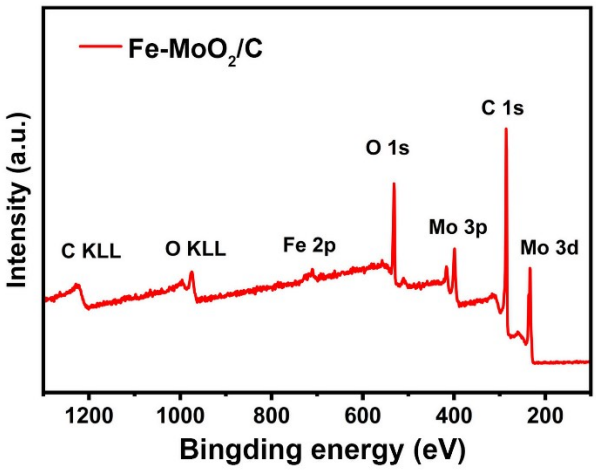

Fig. S2 XPS spectra for Fe-MoO_2/C

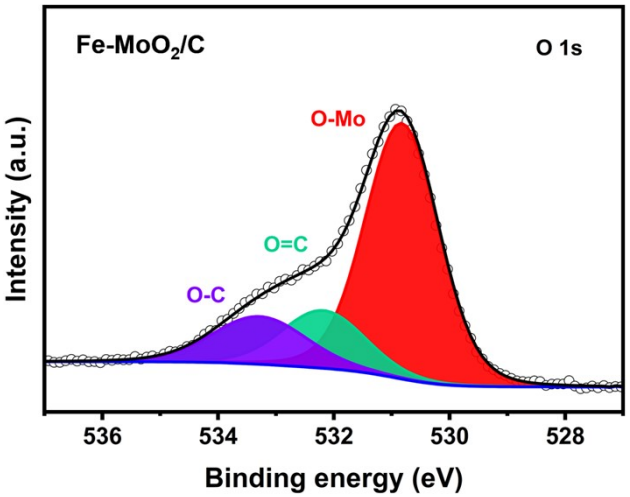

Fig. S3 The O 1s XPS spectra of Fe-MoO_2/C

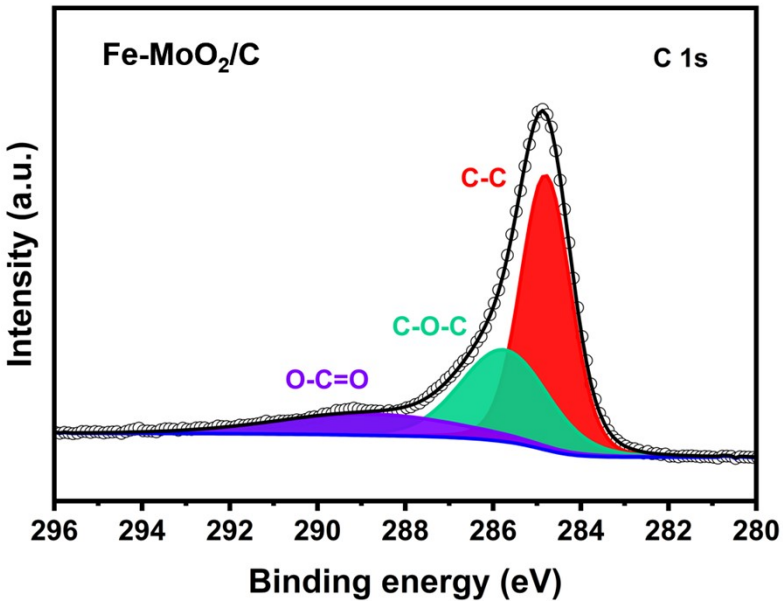

Fig. S4 The C 1s XPS spectra of Fe-MoO_2/C

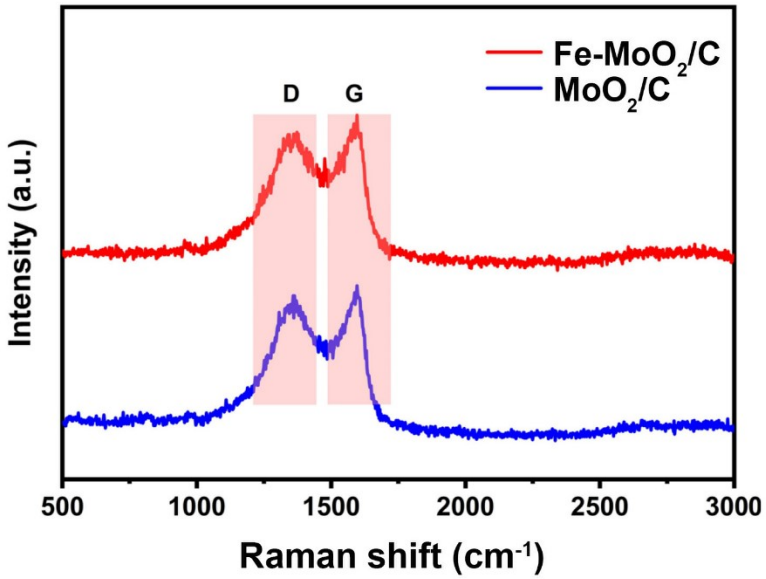

Fig. S5 The Raman spectra of Fe-MoO_2/C and MoO_2/C

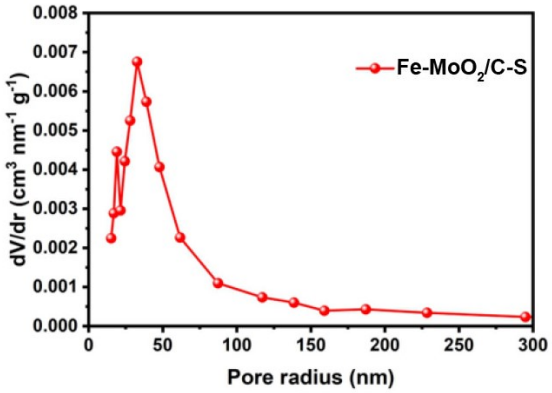

Fig. S6 The pore size distribution of Fe-MoO_2/C-S

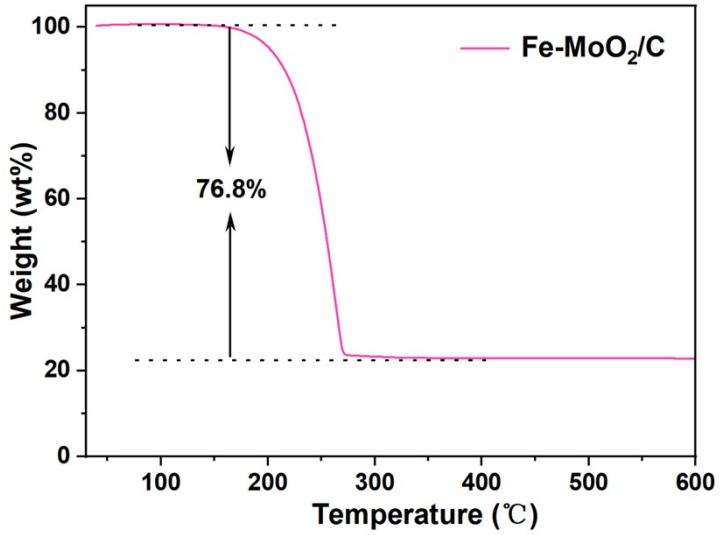

Fig. S7 The TGA analysis of the Fe-MoO_2/C-S and MoO_2/C-S cathodes.

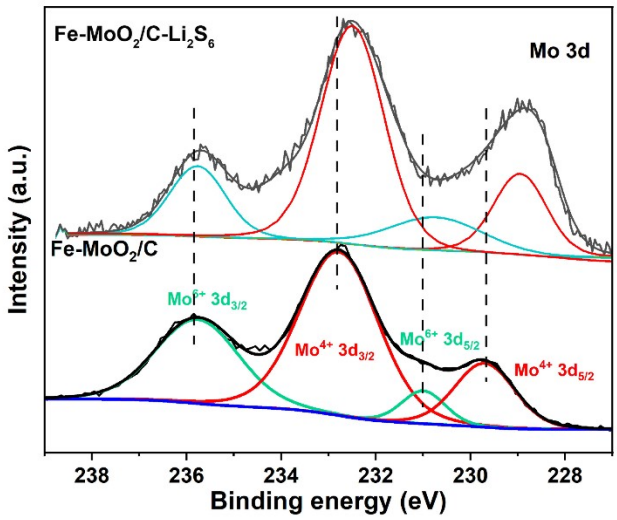

Fig. S8 The Mo 3d XPS spectra of Fe–MoO_2/C both before and after Li_2S_6 adsorption.

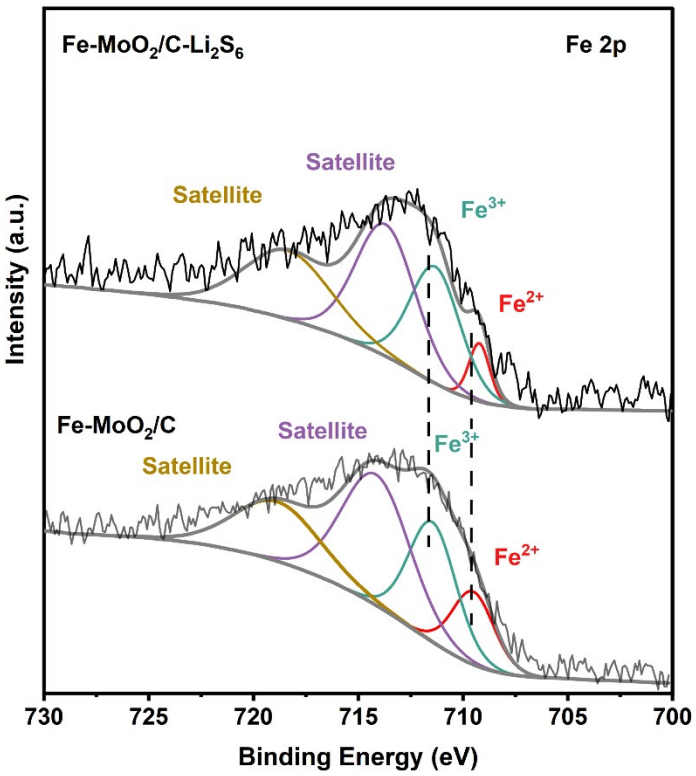

Fig. S9 The Fe 2p XPS spectra of Fe–MoO_2/C both before and after Li_2S_6 adsorption.

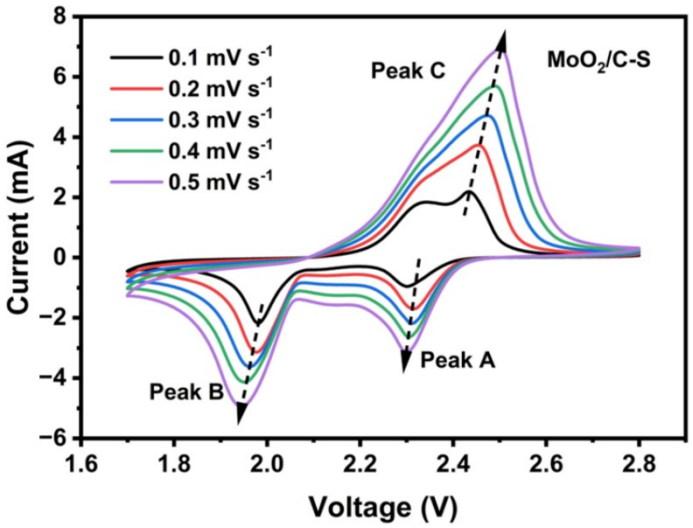

Fig. S10 The CV curves at scanning rates from 0.1 to 0.5 mV s^{-1} of Fe-MoO_2/C.

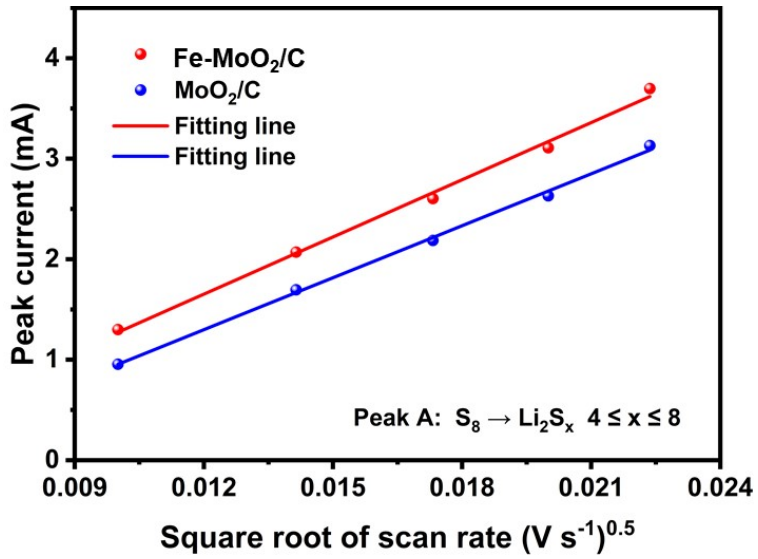

Fig. S11 The relationship between the peak A current and the square root of the scanning rate corresponding to the CV curves of the two electrodes.

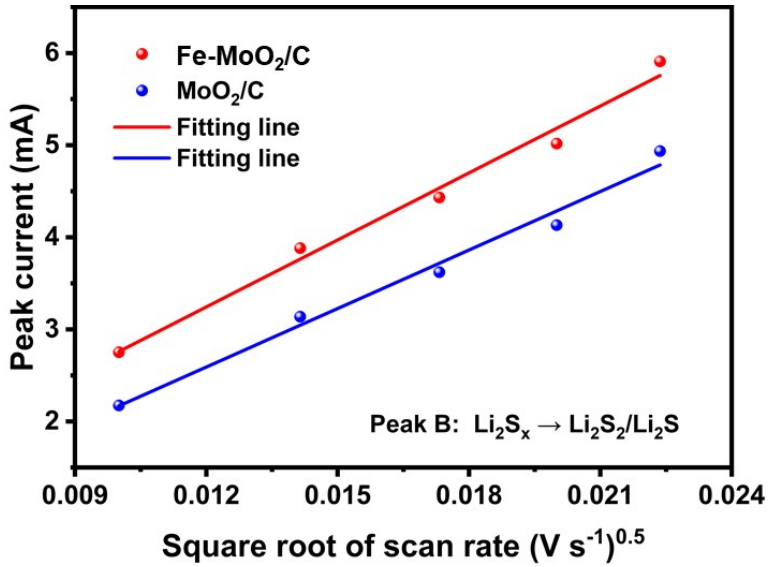

Fig. S12 The relationship between the peak B current and the square root of the scanning rate corresponding to the CV curves of the two electrodes.

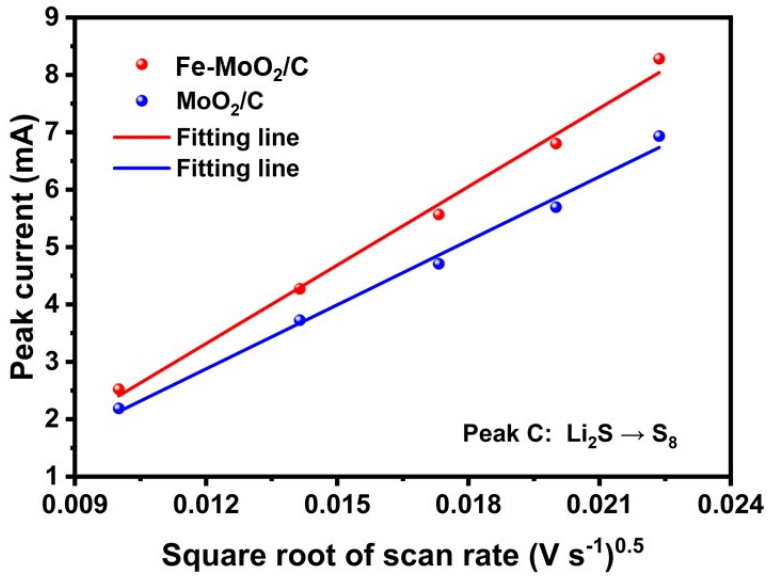

Fig. S13 The relationship between the peak C current and the square root of the scanning rate corresponding to the CV curves of the two electrodes.

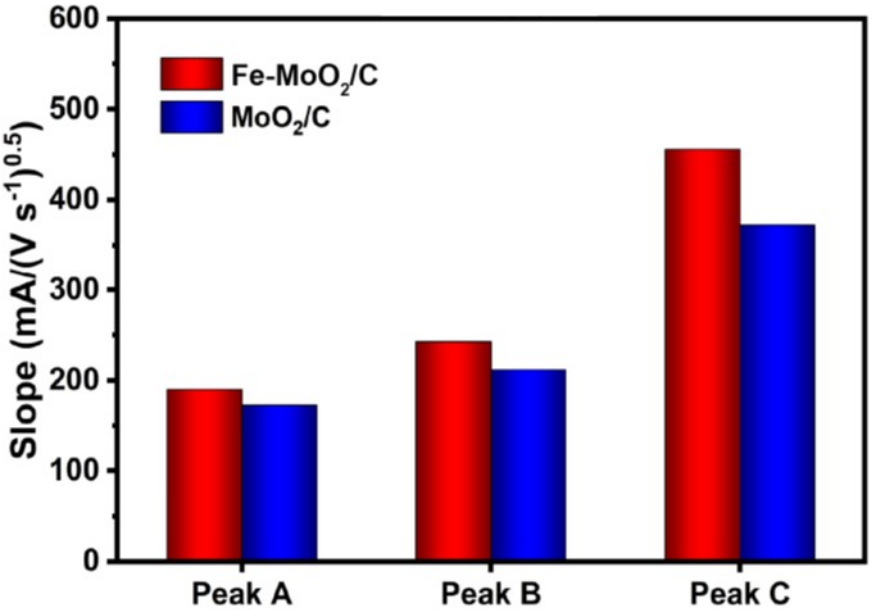

Fig. S14 Bar graph showing slopes for different peaks

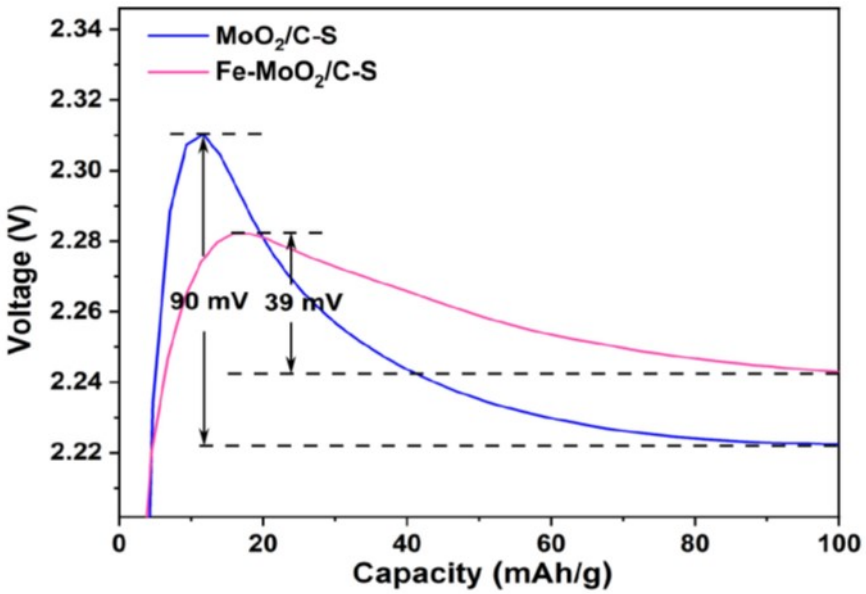

Fig. S15 Enlarged view of a section of the charge–discharge curves of Fe-MoO_2/C-S and MoO_2/C-S

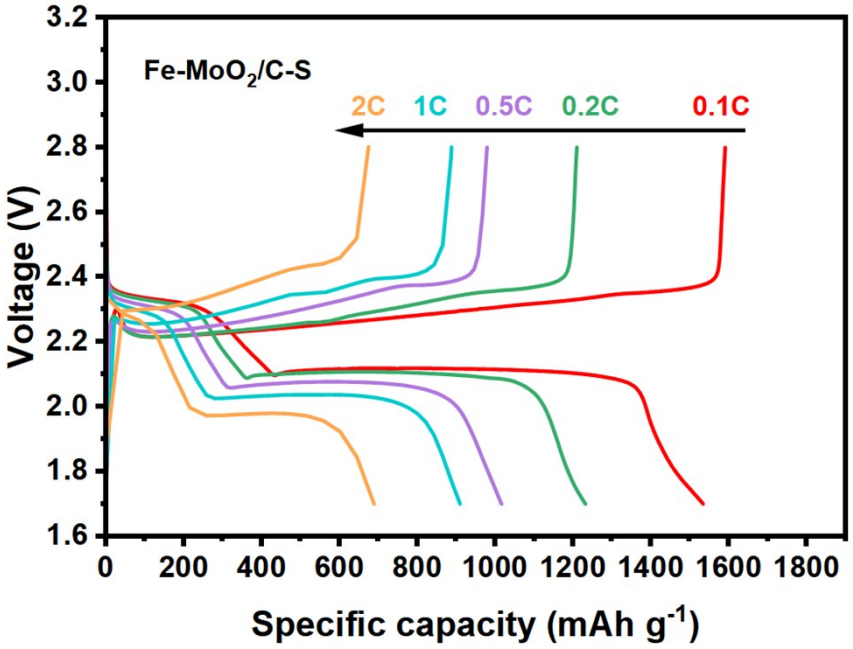

Fig. S16 Charge-discharge patterns of Fe-MoO_2/C cathodes at different current density.

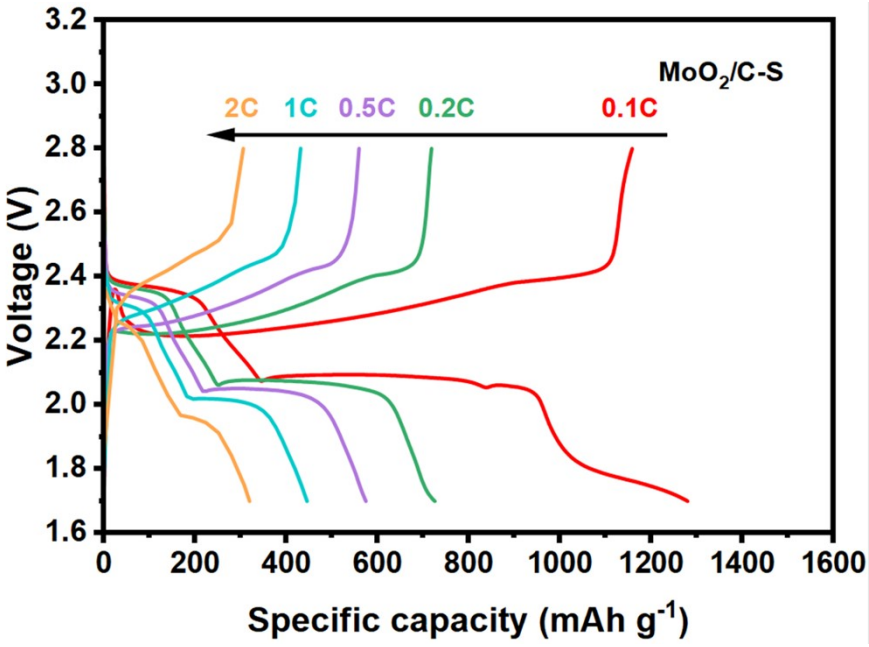

Fig. S17 Charge-discharge patterns of MoO_2/C cathodes at different current density.

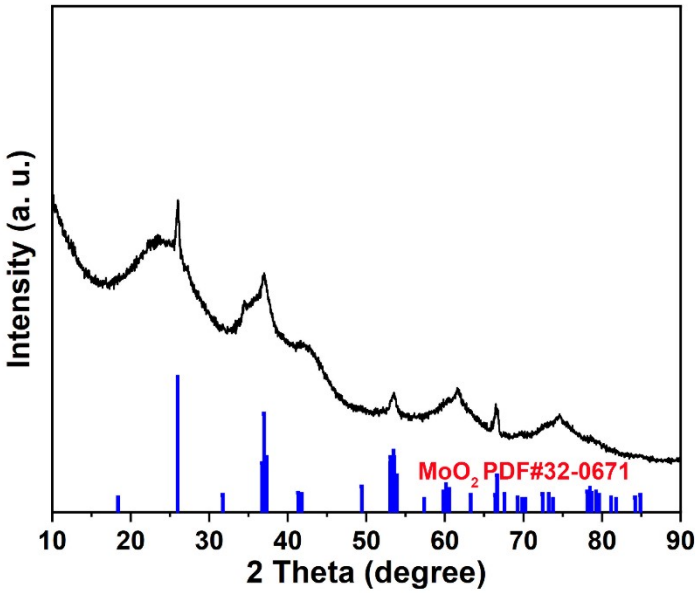

Fig. S18 The XRD images of the cycled cathode